Supporting Information

Advanced 3D Hollow-Out ZnZrO@C Combined with Hierarchical Zeolite for Highly Active and Selective CO Hydrogenation to Aromatics

Yajing Wang,[a] Weiteng Zhan,[a] Zhijie Chen,[a] Jianmin Chen,[a] Xingang Li,[b,*] and Yingwei Li[a,*]

[a] State Key Laboratory of Pulp and Paper Engineering, School of Chemistry and Chemical Engineering, South China University of Technology, Guangzhou 510640, China.

[b] Collaborative Innovation Center for Chemical Science & Engineering (Tianjin), State Key Laboratory of Chemical Engineering, Tianjin Key Laboratory of Applied Catalysis Science & Engineering, School of Chemical Engineering and Technology, Tianjin University, Tianjin 300072, China.

* Corresponding authors

E-mail: liyw@scut.edu.cn, xingang_li@tju.edu.cn

Table S1. Textural features of UiO-66 and MTV-UiO-66 samples.

Sample	S_{BET}[a] ($m^2\ g^{-1}$)	S_{micro}[b] ($m^2\ g^{-1}$)	S_{meso}[c]/ S_{micro}	V_t[d] ($cm^3\ g^{-1}$)	V_{micro}[e] ($cm^3\ g^{-1}$)	V_{meso}[f]/ V_{micro}
UiO-66	826.9	754.8	0.09	0.45	—	—
MTV-UiO-66($Zn_{0.010}Zr_{0.990}$)	622.3	509.3	0.22	0.41	0.26	0.57
MTV-UiO-66($Zn_{0.021}Zr_{0.979}$)	784.3	635.4	0.23	0.57	0.32	0.78
MTV-UiO-66($Zn_{0.040}Zr_{0.960}$)	791.3	491.2	0.61	1.08	0.26	3.11
MTV-UiO-66($Zn_{0.178}Zr_{0.822}$)	490.3	181.3	1.70	0.62	0.09	5.46

[a] Specific surface area was calculated by using the BET method.

[b] Specific micropore surface area was calculated by t-Plot.

[c] Specific mesopore surface area was calculated by subtracting S_{micro} from S_{BET}.

[d] Total specific pore volume was calculated by using the adsorption branch of the N_2 isotherm at $P/P_0 = 0.95$.

[e] Specific micropore volume was calculated by t-Plot.

[f] Specific mesopore volume was calculated by subtracting V_{micro} from V_t.

Table S2. Elemental analysis of the MTV-UiO-66(Zn_xZr_{1-x}) samples with different substitution content of Zn-SBUs.

Sample	Zn:Zr atomic ratio	
	EDX	ICP-OES
MTV-UiO-66($Zn_{0.010}Zr_{0.990}$)	1.1 : 98.9	1.0 : 86.9
MTV-UiO-66($Zn_{0.021}Zr_{0.979}$)	2.1 : 97.9	1.0 : 47.1
MTV-UiO-66($Zn_{0.040}Zr_{0.960}$)	4.3: 95.7	1.0 : 22.0
MTV-UiO-66($Zn_{0.178}Zr_{0.822}$)	17.8 : 82.2	1.0 : 7.6

For simplicity, the MTV-UiO-66($Zn_{0.021}Zr_{0.979}$) was denoted as MTV-UiO-66(ZnZr)

Table S3. Structural properties of ZrO_2@C, HO-ZnZrO@C, and $Zn_xZr_{1-x}O$@C samples.

Sample	S_{BET} ($m^2\ g^{-1}$)	S_{micro} ($m^2\ g^{-1}$)	S_{meso}/S_{micro}	V_t ($cm^3\ g^{-1}$)	V_{micro} ($cm^3\ g^{-1}$)	V_{meso}/V_{micro}
ZrO_2@C	130.9	60.1	1.2	0.128	0.032	3.0
$Zn_{0.010}Zr_{0.990}O$@C	91.3	29.8	2.1	0.188	0.016	10.8
HO-ZnZrO@C	86.3	15.0	4.8	0.156	0.007	21.3
$Zn_{0.040}Zr_{0.960}O$@C	113.8	16.7	5.8	0.247	0.008	29.9
$Zn_{0.178}Zr_{0.822}O$@C	192.9	38.2	4.1	0.207	0.018	10.5

Table S4. H-ZSM-5 treated with different concentrations of NaOH.

NaOH concentration (M)	S_{BET} (m^2 g^{-1})	S_{micro} (m^2 g^{-1})	S_{meso}/ S_{micro}	V_t (cm^3 g^{-1})	V_{micro} (cm^3 g^{-1})	V_{meso}/ V_{micro}
0	293.7	236.7	0.24	0.161	0.121	0.33
0.1	318.9	237.4	0.34	0.179	0.122	0.47
0.6	302.6	164.9	0.83	0.355	0.084	3.23
1.0	264.9	139.5	0.90	0.324	0.074	3.32

Table S5. Comparison of productivities for methanol-intermediated CO_x hydrogenation to aromatics.

Catalyst	Oxide/Zeolite (weight ratio)	Reactant	P (MPa)	Temp. (°C)	GHSV (mL g_{cat}^{-1} h^{-1})	X_{COx} (%)	$S_{aromatics}$ (%)	Aromatics STY (g g_{oxide}^{-1} h^{-1})	Ref.
HO-ZnZrO@C/Z5-0.6	2/1[a]	CO + H_2	3	360	1200	42.6	58.6	0.081	This work
HO-ZnZrO@C/Z5-0.6	2/1[a]	CO + H_2	3	360	2400	39.5	67.5	0.175	This work
HO-ZnZrO@C/Z5-0.6	2/1[a]	CO + H_2	3	360	3600	35.2	73.1	0.261	This work
HO-ZnZrO@C/Z5-0.6	2/1[a]	CO + H_2	3	360	4800	28.1	74.3	0.282	This work
HO-ZnZrO@C/Z5-0.6	2/1[a]	CO + H_2	3	360	6000	24.3	72.8	0.302	This work
HO-ZnZrO@C/Z5-0.6	2/1[a]	CO + H_2	3	360	7200	19.8	70.1	0.286	This work
B-ZnZrO/Z5-0.6	2/1	CO + H_2	3	360	3600	16.1	38.8	0.045	This work
Mo-ZrO_2/H-ZSM-5	1/2	CO + H_2	4	400	3000	22.0	76.0	0.165	1
$Ce_{0.2}Zr_{0.8}O_2$/HZSM-5	1/1	CO + H_2	2	450	600	22.4	56.3	0.028	2
ZrO_2-400&H-ZSM-5	2/1	CO + H_2	6	350	1000	11.6	62.3	0.018	3

Zn-ZrO_2/H-ZSM-5	1/2	$CO + H_2$	4	430	1500	23	80	0.028	4
ZnZrO/ZSM-5	1/1	$CO_2 + H_2$	4	320	1200	14	73	0.027	5
ae-ZnO–ZrO_2/ZSM-5	1/2	$CO_2 + H_2$	4	340	7200	15.9	76.0	0.239	6
ZnO/ZrO_2+ZSM-5	1/2	$CO_2 + H_2$	3	340	2700	9.1	70	0.036	7
Cr_2O_3/H-ZSM-5	1/1	$CO_2 + H_2$	3	350	1200	34.5	75.9	0.077	8
Cr_2O_3/Zn-ZSM-5@SiO_2	1/2	$CO_2 + H_2$	3	350	1200	22.1	70.1	0.056	9
$ZnCrO_x$–ZSM-5-533	1/1	$CO + H_2$	4	350	1500	16	74	0.050	10
$ZnCrO_x$-ZnZSM-5	1/1	$CO_2 + H_2$	5	320	2000	19.9	56.5	0.019	11
$ZnAlO_x$&H-ZSM-5	1/1	$CO_2 + H_2$	3	320	2000	9.1	73.9	0.017	12

[a] $W_{(HO\text{-}ZnZrO@C)}/W_{(Z5\text{-}0.6)}$ = 2/1, the weight ratio of C in HO-ZnZrO@C was determined to be 14%.

Table S6. Structural properties of selected samples.

Sample	S_{BET} ($m^2\ g^{-1}$)	S_{micro} ($m^2\ g^{-1}$)	S_{meso}/S_{micro}	V_t ($cm^3\ g^{-1}$)	V_{micro} ($cm^3\ g^{-1}$)	V_{meso}/V_{micro}
HO-ZnZrO@C+Z5-0.6	171.0	75.4	1.27	0.193	0.038	3.95
HO-ZnZrO@C/Z5-0.6	170.1	74.7	1.28	0.207	0.038	4.53

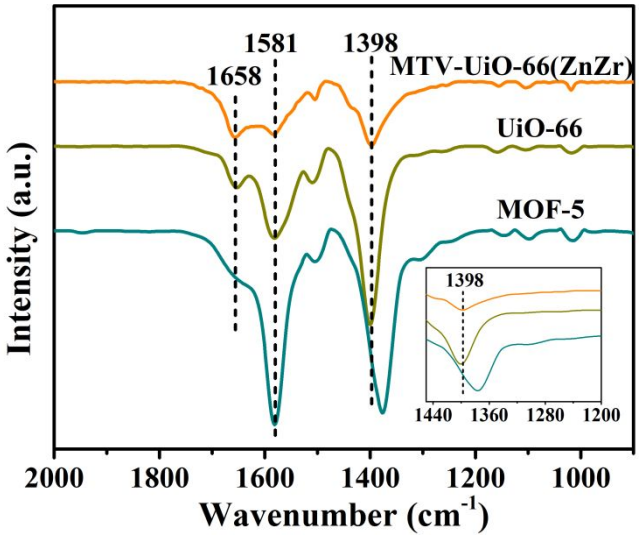

Figure S1. FT-IR spectra of the MTV-UiO-66(ZnZr), UiO-66, and MOF-5.

As presented in the FT-IR spectra, the IR bands at about 1581 and 1398 cm^{-1} were assigned to asymmetric and symmetric vibrations of the carboxyl groups, respectively. The IR band at 1658 cm^{-1} was ascribed to the ν(C=O) vibration of DMF. Note that the band corresponding to asymmetric (OCO) vibration of MTV-UiO-66(ZnZr) located between those of pure UiO-66 and MOF-5, which implied the changes of the coordination environment between carboxylate groups and metal ions within the MTV-UiO-66(ZnZr) framework in comparison with that of pure UiO-66, due to the incorporation of Zn oxide clusters.

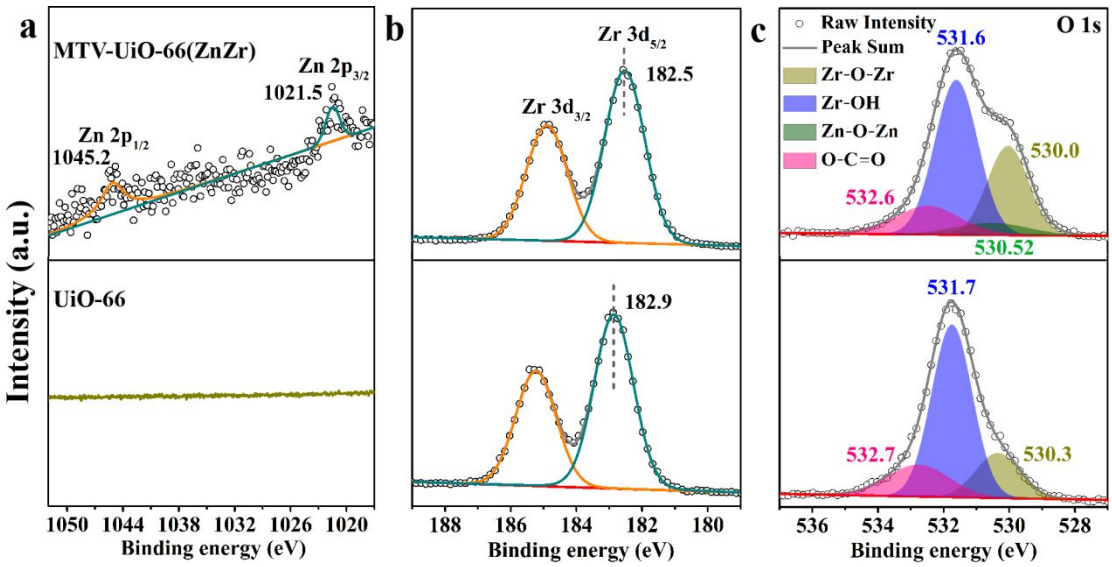

Figure S2. High-resolution (a) Zn 2p, (b) Zr 3d, and (c) O 1s XPS spectra of MTV-UiO-66(ZnZr) and UiO-66.

XPS was employed to evaluate the surface chemical composition and electronic structure. In the high-resolution Zn XPS spectra, the doublet spectral lines of Zn 2p exhibited a spin–orbit splitting value of 23 eV, indicative of the presence of Zn^{2+}.[13] As shown in the high-resolution Zr XPS spectra, all samples possessed doublet spectral lines of Zr $3d_{5/2}$ and Zr $3d_{3/2}$, the area ratios of which were 3 : 2, with a spin-orbit splitting of 2.4 eV. Those observations suggest that Zr^{4+} was exclusively formed.[14] It is worth noting that the Zr 3d binding energy of MTV-UiO-66(ZnZr) took a slight down-shift in comparison with that of pure UiO-66, demonstrating the modified local electronic structure of Zr within MTV-UiO-66(ZnZr). As compared with pure UiO-66, the O spectra of MTV-UiO-66(ZnZr), which could be divided into four peaks corresponding to Zr-O-Zr, Zr-OH, Zn-O-Zn, and O-C=O,[15] were negatively shifted. These results strongly suggest that the localized Zr-SBUs within the MTV-UiO-66 framework have been partially replaced by Zn-SBUs.

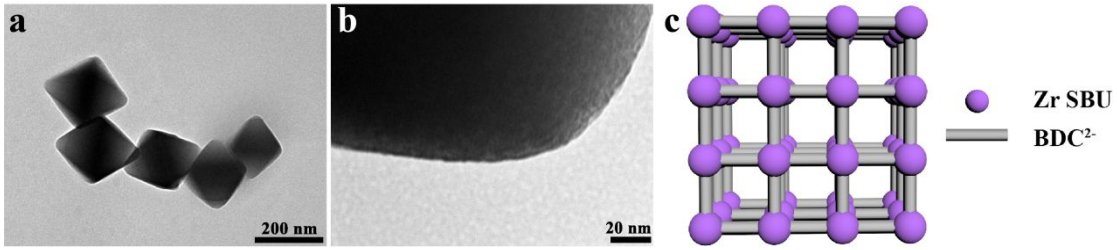

Figure S3. (a,b) TEM images and (c) structure of UiO-66.

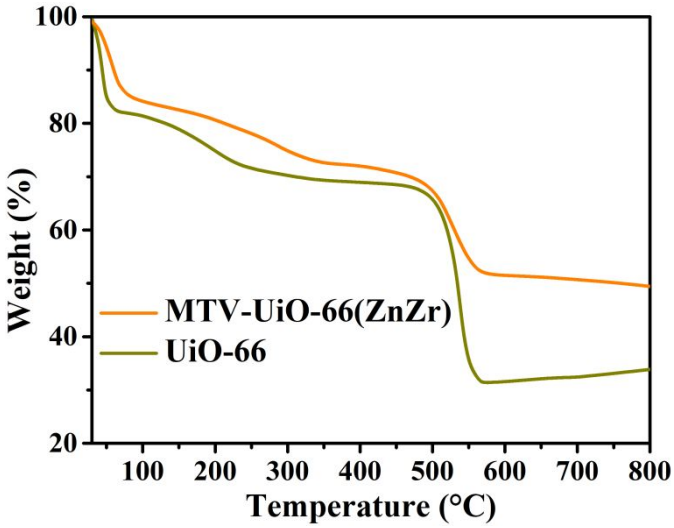

Figure S4. TG profiles taken for MTV-UiO-66(ZnZr) and UiO-66 in N_2 atmosphere.

According to the TG analysis, as compared with pure UiO-66, the thermal stability of MTV-UiO-66(ZnZr) compromised slightly, as a result of MTV-UiO-66(ZnZr) with lower network connections, associated with the introduction of Zn-SBUs. Finally, the pyrolysis temperature of MTV-UiO-66(ZnZr) was determined to be 600 °C in inert atmosphere for complete carbonization of organic ligands.

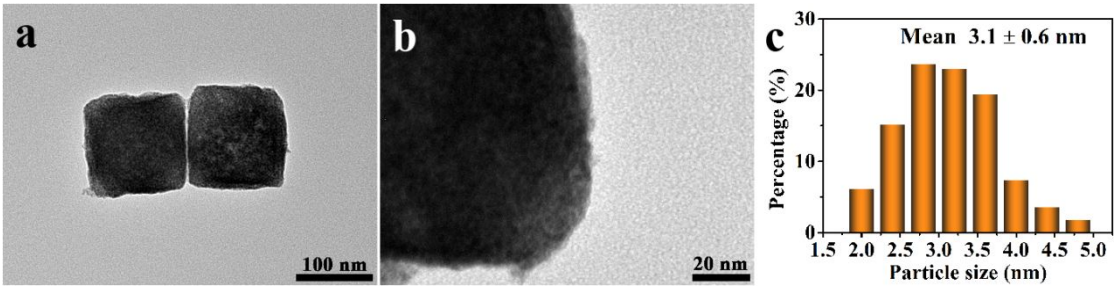

Figure S5. (a,b) TEM images and (c) corresponding ZrO_2 particle size distributions of ZrO_2@C.

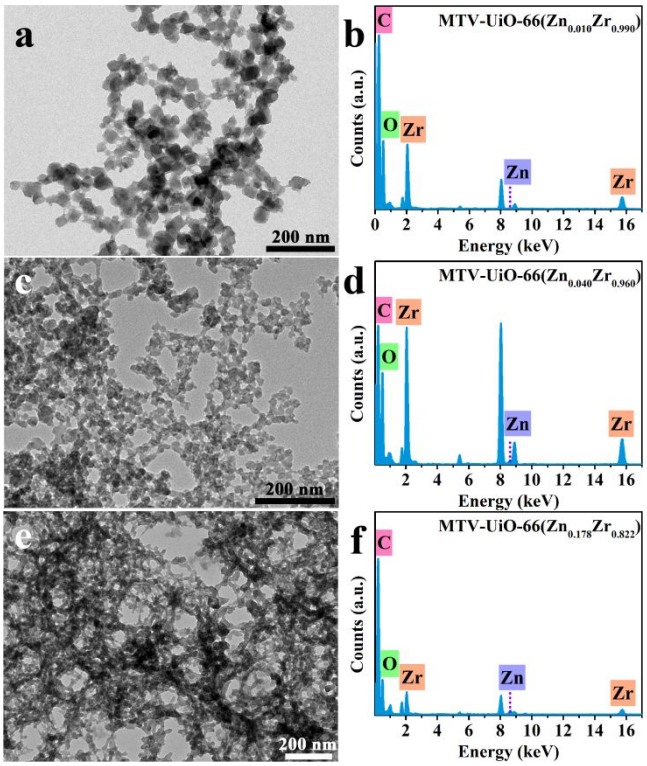

Figure S6. (a,c,e) TEM images and (b,d,f) corresponding elemental spectra for (a,b) MTV-UiO-66($Zn_{0.010}Zr_{0.990}$), (c,d) MTV-UiO-66($Zn_{0.040}Zr_{0.960}$), and (e,f) MTV-UiO-66($Zn_{0.178}Zr_{0.822}$), respectively.

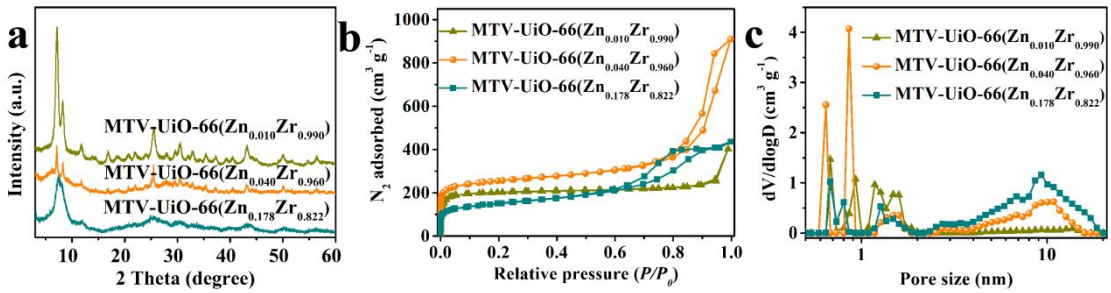

Figure S7. (a) XRD patterns, (b) N_2 adsorption-desorption isotherms, and (c) pore size distributions for MTV-UiO-66(Zn_xZr_{1-x}) (x = 0.010, 0.040, and 0.178).

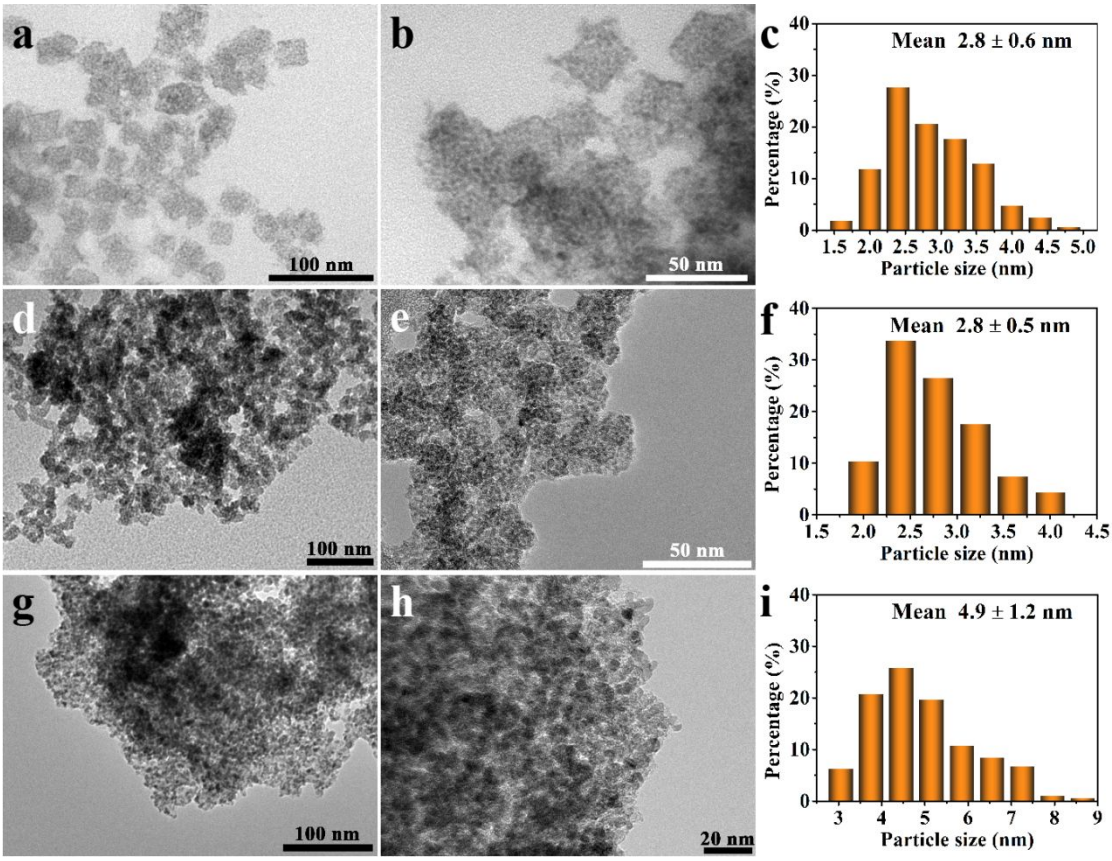

Figure S8. (a,d,g) TEM images, (b,e,h) high-magnification TEM images, and (c,f,i) ZnZrO particle size distributions for (a,b,c) $Zn_{0.010}Zr_{0.990}O@C$, (d,e,f) $Zn_{0.040}Zr_{0.960}O@C$, and (g,h,i) $Zn_{0.178}Zr_{0.822}O@C$.

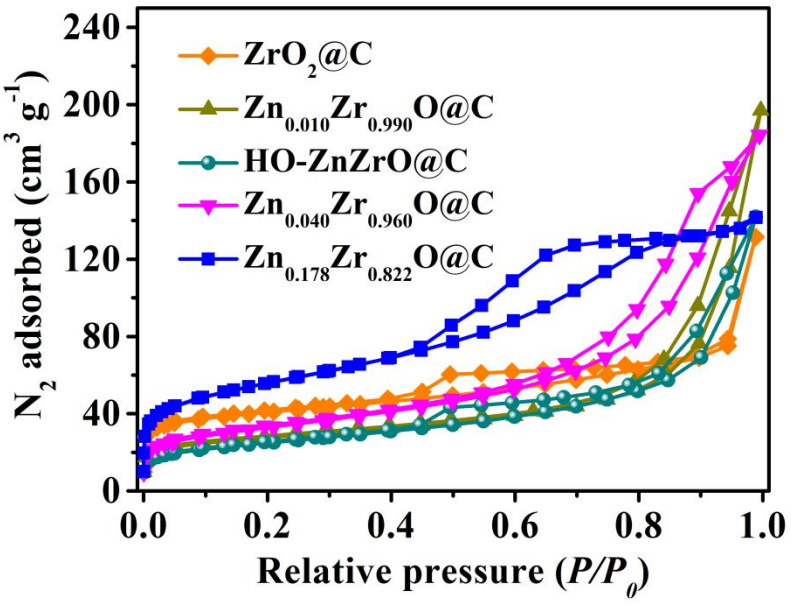

Figure S9. N_2 adsorption-desorption isotherms for ZrO_2@C, HO-ZnZrO@C, and $Zn_xZr_{1-x}O$@C (x = 0.010, 0.040, and 0.178).

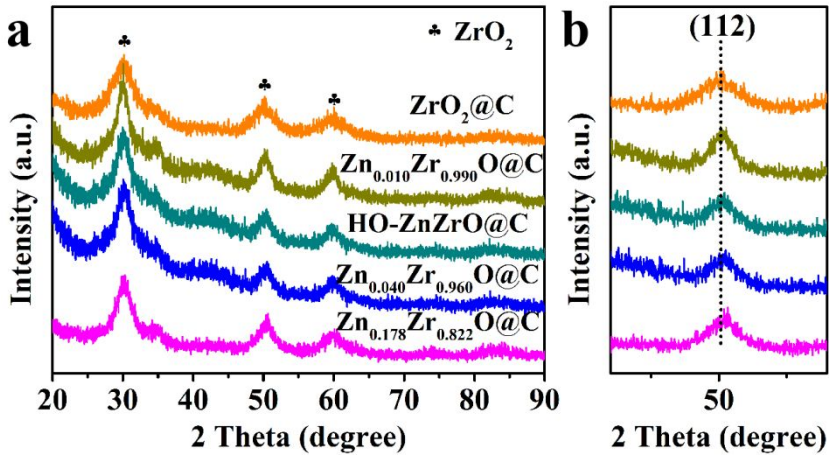

Figure S10. (a) XRD patterns and (b) enlarged XRD patterns for ZrO_2@C, HO-ZnZrO@C, and $Zn_xZr_{1-x}O$@C (x = 0.010, 0.040, and 0.178).

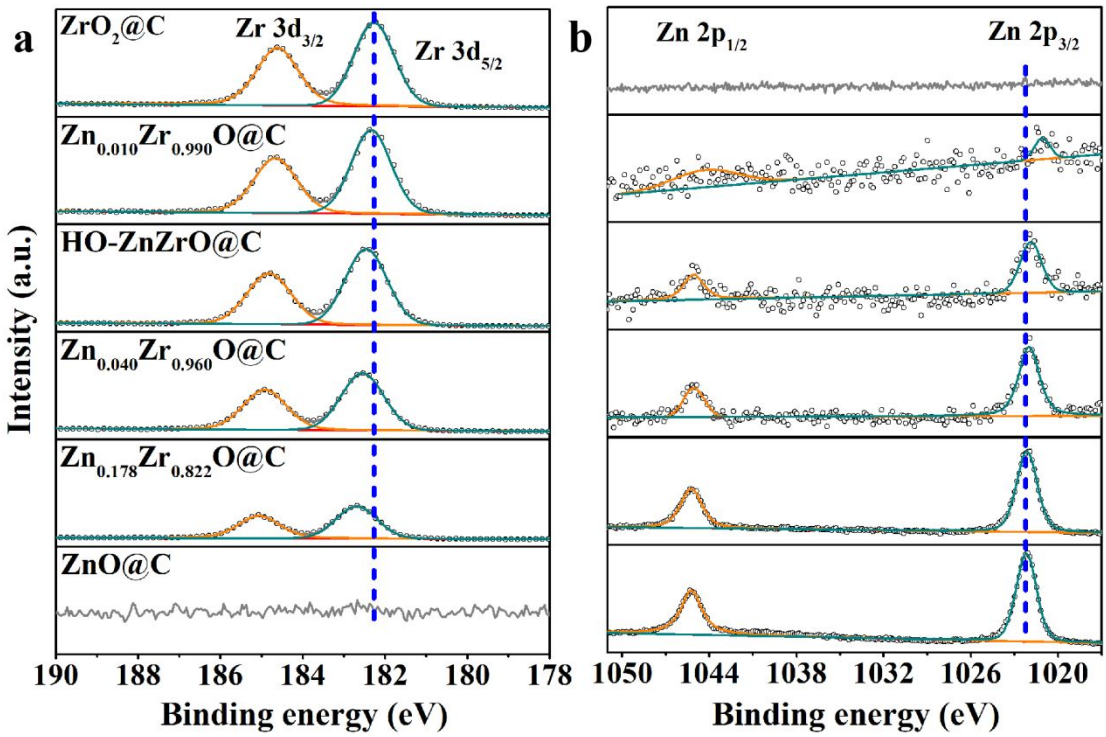

Figure S11. XPS spectra of the ZrO_2@C, HO-ZnZrO@C, $Zn_xZr_{1-x}O$@C (x = 0.010, 0.040, and 0.178), and ZnO@C. (a) Zr 3d and (b) Zn 2p.

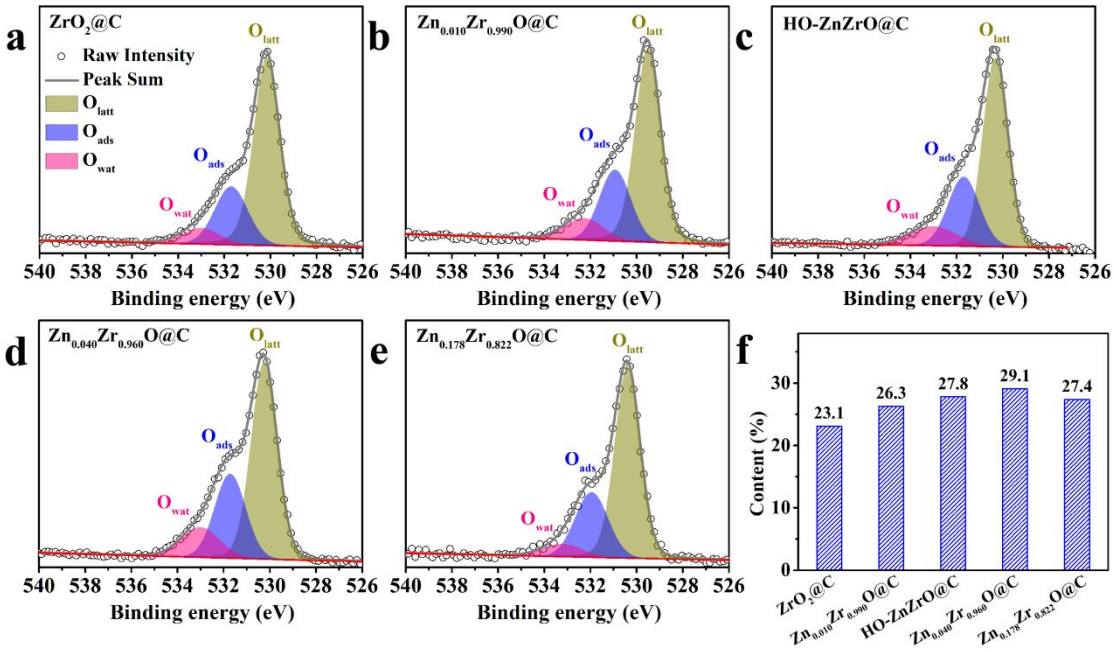

Figure S12. O 1s XPS spectra of (a) ZrO_2@C, (b) $Zn_{0.010}Zr_{0.990}O$@C, (c) HO-ZnZrO@C, (d) $Zn_{0.040}Zr_{0.960}O$@C, (e) $Zn_{0.178}Zr_{0.822}O$@C, and (f) the relative content of surface oxygen species in all O species of the samples. HO-ZnZrO@C represents HO-$Zn_{0.021}Zr_{0.979}O$@C.

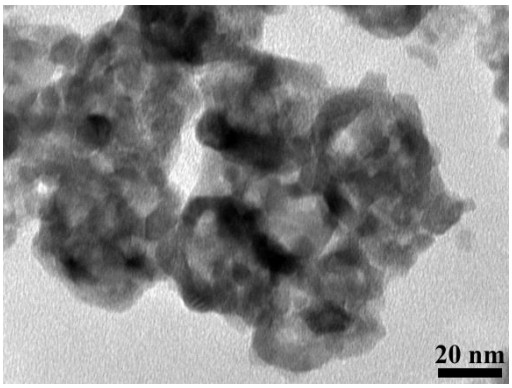

Figure S13. TEM image of the HO-ZnZrO@C obtained at 600 °C for 10 h in Ar atmosphere.

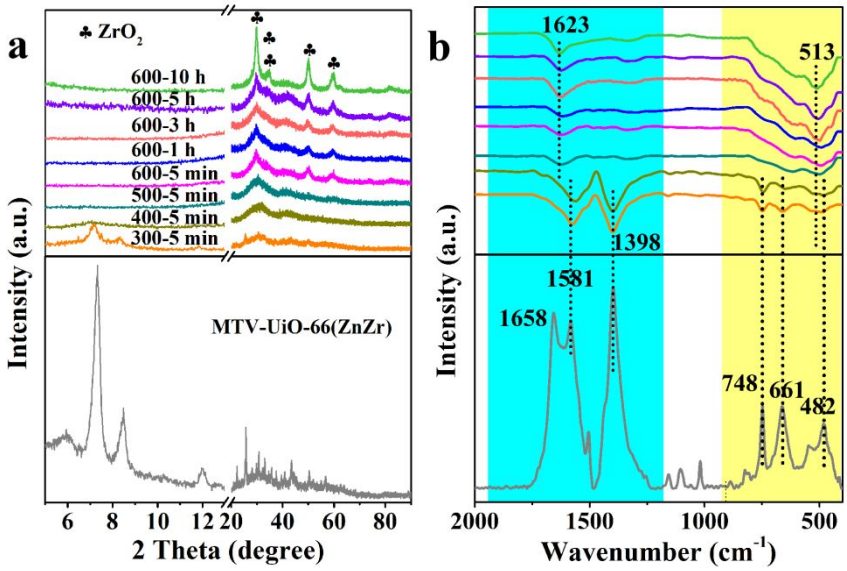

Figure S14. (a) XRD patterns and (b) FT-IR spectra for the samples obtained from thermolysis of MTV-UiO-66(ZnZr) under different temperature and time in Ar flow.

As shown in Figure S13b, when the carbonization temperature was increased from room temperature to 400 °C, the characteristic peaks corresponding to the asymmetric (OCO) and symmetric (OCO) variations of carboxylate species, showed slight red shifts as compared with those (at 1581 and 1398 cm^{-1}) of MTV-UiO-66(ZnZr), indicative of the variation of coordination bonds between carboxyl groups and Zr oxide clusters. The absence of peak at 1658 cm^{-1} implies the elimination of DMF solvent. Moreover, the reduced intensity of peak at 482 cm^{-1} corresponding to ν(μ3-OH) evidenced the transition from $Zr_6O_4(OH)_4$ to Zr_6O_6 cluster.[16] When the pyrolysis temperature was enhanced to 500 °C, the BDC ligands were completely decomposed and ZnZrO particles were formed, as confirmed by the loss of carboxylate bands and the appearance of bands at 1623 (H–O–H) and 513 cm^{-1} (metal–O).[17] The phase and structure transformation process as revealed by the XRD

and FT-IR results is consistent with the observation of TEM characterization as depicted in Figure 4.

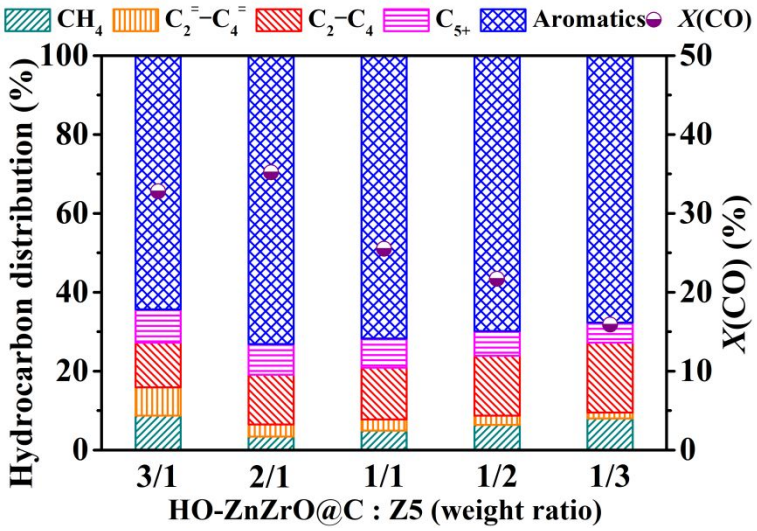

Figure S15. Effect of weight ratio of HO-ZnZrO@C to Z5-0.6 on the CO hydrogenation to aromatics. Reaction conditions: 360 °C, 3.0 MPa, 3600 mL g^{-1} h^{-1}, $H_2/CO = 2$. C_{5+} products exclude aromatics.

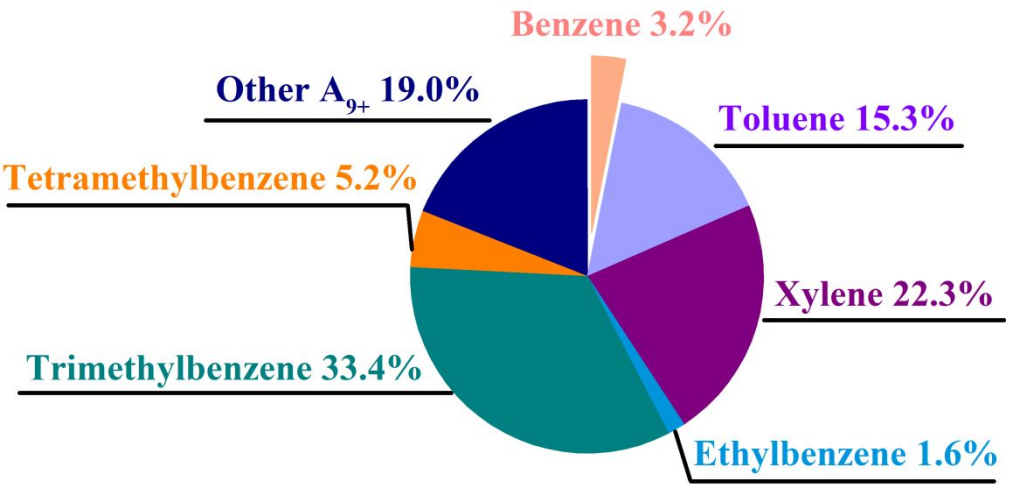

Figure S16. Distribution of aromatic hydrocarbons over the HO-ZnZrO@C/Z5-0.6 catalyst. Other A_{9+}: aromatic hydrocarbons with nine or more than nine carbon atoms except trimethylbenzene and tetramethylbenzene.

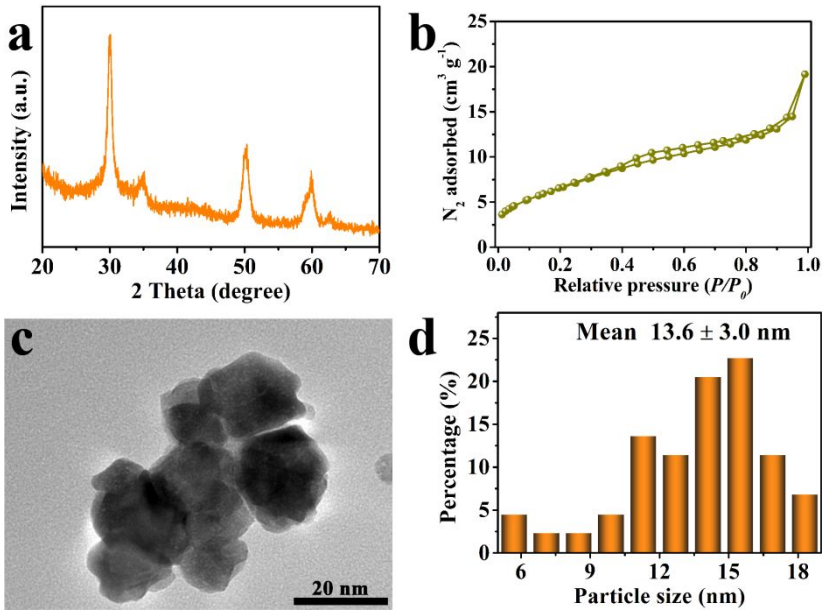

Figure S17. (a) XRD pattern, (b) N_2 adsorption-desorption isotherm, (c) TEM image, and (d) ZnZrO particle size distribution for B-ZnZrO.

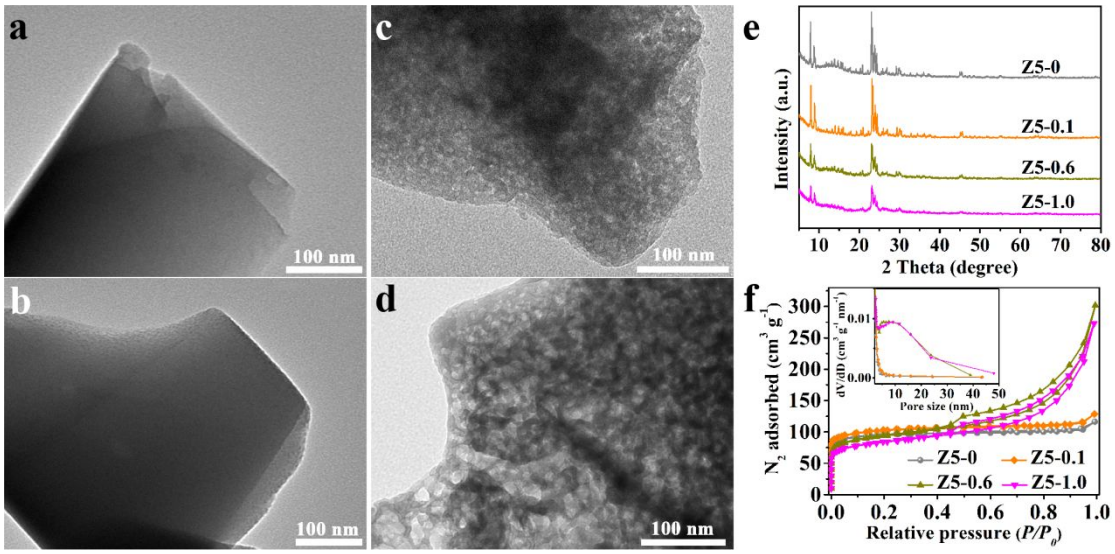

Figure S18. TEM images of (a) Z5-0, (b) Z5-0.1, (c) Z5-0.6, and (d) Z5-1.0. (e) XRD patterns and (f) N_2 adsorption-desorption isotherms and corresponding BJH pore size distributions (insert) for Z5-n.

H-ZSM-5, as a classical zeolite, can be used as catalyst for the synthesis of aromatics, gasoline, and diesel oil from methanol or syngas. Unfortunately, the microporous channels could impede both mass transfer and the accessibility of active sites, leading to the formation of undesirable products and accelerated deactivation of catalysts due to the coke deposition or pore blockage. Thus, it is extremely essential that the secondary pore systems, such as mesoporosity, within microporous H-ZSM-5 are created to improve the catalytic activity and stability.

The pristine H-ZSM-5 was treated by NaOH solutions to create hierarchically porous structures. As observed in the XRD patterns in Figure S17e, all the samples maintained the characteristic diffraction patterns of the MFI structure, however, the diffraction intensities were decreased with an increase in the concentration of NaOH

solutions. The TEM images revealed that the Z5 samples treated by NaOH whose concentration was above 0.6 M possessed obvious mesopores, in accordance with the results of N_2 adsorption/desorption measurements and corresponding BJH pore size distributions.

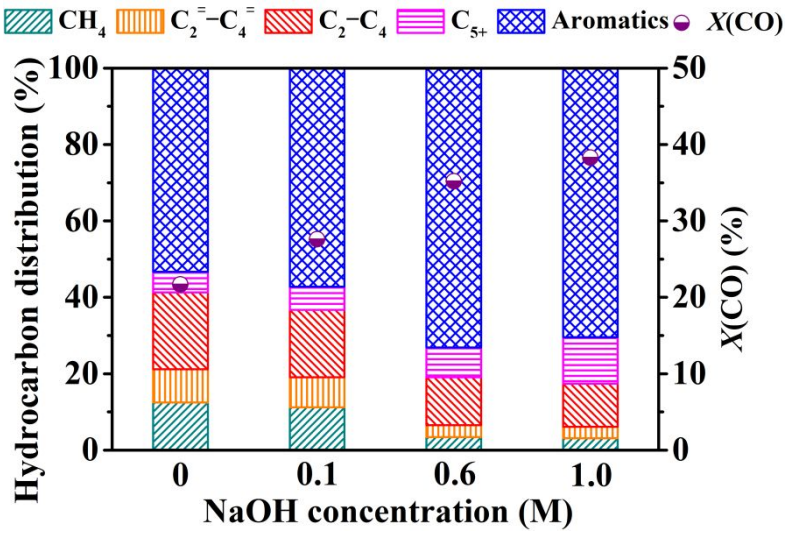

Figure S19. Catalytic performance in CO hydrogenation to aromatics over HO-ZnZrO@C combined with Z5 treated by NaOH solutions with different concentrations. Reaction conditions: 360 °C, 3.0 MPa, 3600 mL g^{-1} h^{-1}, H_2/CO = 2, $W_{(HO\text{-}ZnZrO@C)}/W_{(Z5\text{-}n)}$ = 2/1. C_{5+} products exclude aromatics.

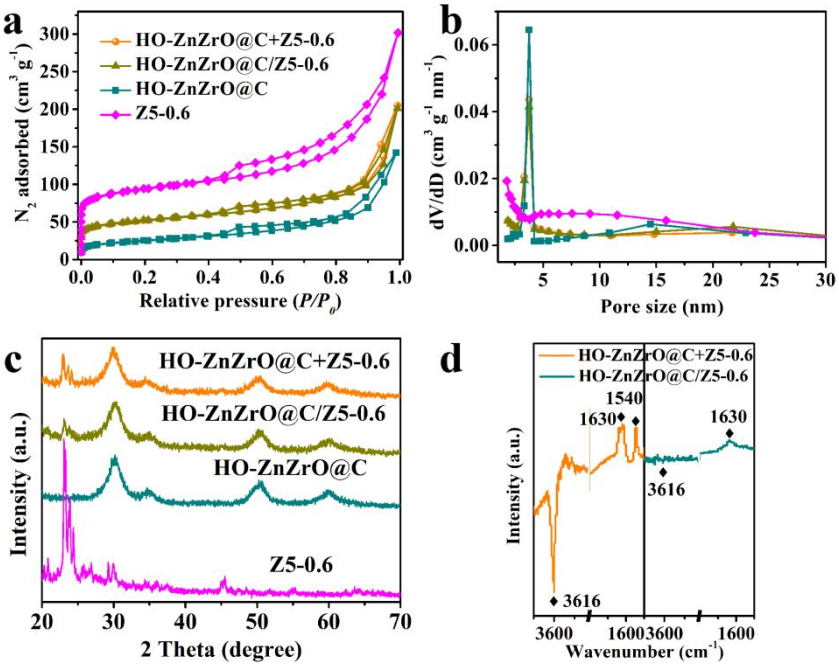

Figure S20. (a) N_2 adsorption-desorption isotherms, (b) BJH pore size distributions, (c) XRD patterns, and (d) 2,6-DTBPy-FTIR spectra collected on HO-ZnZrO@C, Z5-0.6, HO-ZnZrO@C/Z5-0.6, and HO-ZnZrO@C+Z5-0.6.

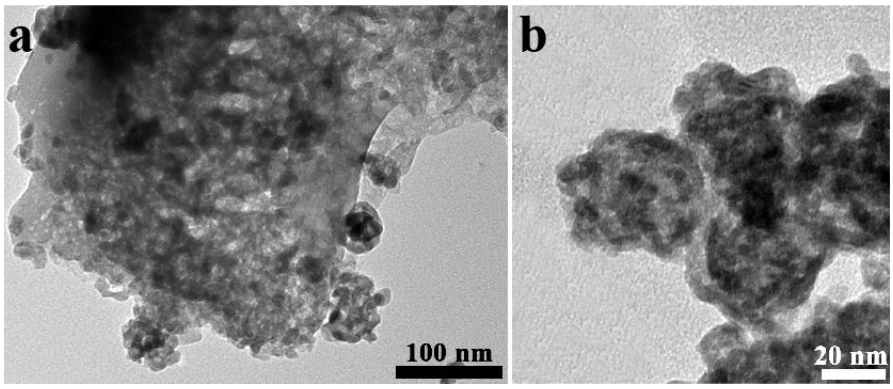

Figure S21. TEM images of the used HO-ZnZrO@C/Z5-0.6 catalyst after 200 h of reaction.

REFERENCES

(1) Zhou, W.; Shi, S.; Wang, Y.; Zhang, L.; Wang, Y.; Zhang, G.; Min, X.; Cheng, K.; Zhang, Q.; Kang, J.; Wang, Y. Selective Conversion of Syngas to Aromatics over a Mo−ZrO_2/H‐ZSM‐5 Bifunctional Catalyst. *ChemCatChem* **2019,** *11*, 1681-1688.

(2) Huang, Z.; Wang, S.; Qin, F.; Huang, L.; Yue, Y.; Hua, W.; Qiao, M.; He, H.; Shen, W.; Xu, H. Ceria-Zirconia/Zeolite Bifunctional Catalyst for Highly Selective Conversion of Syngas into Aromatics. *ChemCatChem* **2018,** *10*, 4519-4524.

(3) Liu, J.; He, Y.; Yan, L.; Li, K.; Zhang, C.; Xiang, H.; Wen, X.; Li, Y. Nano-Sized ZrO_2 Derived from Metal–Organic Frameworks and Their Catalytic Performance for Aromatic Synthesis from Syngas. *Catal. Sci. Technol.* **2019,** *9*, 2982-2992.

(4) Cheng, K.; Zhou, W.; Kang, J.; He, S.; Shi, S.; Zhang, Q.; Pan, Y.; Wen, W.; Wang, Y. Bifunctional Catalysts for One-Step Conversion of Syngas into Aromatics with Excellent Selectivity and Stability. *Chem* **2017,** *3*, 334-347.

(5) Li, Z.; Qu, Y.; Wang, J.; Liu, H.; Li, M.; Miao, S.; Li, C. Highly Selective Conversion of Carbon Dioxide to Aromatics over Tandem Catalysts. *Joule* **2019,** *3*, 570-583.

(6) Zhou, C.; Shi, J.; Zhou, W.; Cheng, K.; Zhang, Q.; Kang, J.; Wang, Y. Highly Active ZnO-ZrO_2 Aerogels Integrated with H-ZSM-5 for Aromatics Synthesis from Carbon Dioxide. *ACS Catal.* **2019,** *10*, 302-310.

(7) Zhang, X.; Zhang, A.; Jiang, X.; Zhu, J.; Liu, J.; Li, J.; Zhang, G.; Song, C.; Guo, X. Utilization of CO_2 for Aromatics Production over ZnO/ZrO_2-ZSM-5 Tandem Catalyst. *J. CO_2 Util.* **2019,** *29*, 140-145.

(8) Wang, Y.; Tan, L.; Tan, M.; Zhang, P.; Fang, Y.; Yoneyama, Y.; Yang, G.; Tsubaki, N. Rationally Designing Bifunctional Catalysts as an Efficient Strategy to Boost CO_2 Hydrogenation Producing Value-Added Aromatics. *ACS Catal.* **2018,** *9*, 895-901.

(9) Wang, Y.; Gao, W.; Kazumi, S.; Li, H.; Yang, G.; Tsubaki, N. Direct and Oriented Conversion of CO_2 into Value-Added Aromatics. *Chem. Eur. J.* **2019,** *25*, 5149-5153.

(10) Yang, J.; Pan, X.; Jiao, F.; Li, J.; Bao, X. Direct Conversion of Syngas to Aromatics. *Chem. Commun.* **2017,** *53*, 11146-11149.

(11) Zhang, J.; Zhang, M.; Chen, S.; Wang, X.; Zhou, Z.; Wu, Y.; Zhang, T.; Yang, G.; Han, Y.; Tan, Y. Hydrogenation of CO_2 into Aromatics over a $ZnCrO_x$-Zeolite Composite Catalyst. *Chem. Commun.* **2019,** *55*, 973-976.

(12) Ni, Y.; Chen, Z.; Fu, Y.; Liu, Y.; Zhu, W.; Liu, Z. Selective Conversion of CO_2 and H_2 into Aromatics. *Nat. Commun.* **2018,** *9*, 3457.

(13) Zhang, J.; Gao, D.; Yang, G.; Zhang, J.; Shi, Z.; Zhang, Z.; Zhu, Z.; Xue, D. Synthesis and Magnetic Properties of Zr Doped ZnO Nanoparticles. *Nanoscale Res. Lett.* **2011,** *6*, 587.

(14) Tan, Z.; Li, S.; Wang, F.; Qian, D.; Lin, J.; Hou, J.; Li, Y. High Performance Polymer Solar Cells with as-Prepared Zirconium Acetylacetonate Film as Cathode Buffer Layer. *Sci. Rep.* **2014,** *4*, 4691.

(15) Min, X.; Wu, X.; Shao, P.; Ren, Z.; Ding, L.; Luo, X. Ultra-High Capacity of Lanthanum-Doped UiO-66 for Phosphate Capture: Unusual Doping of Lanthanum by the Reduction of Coordination Number. *Chem. Eng. J.* **2019,** *358*, 321-330.

(16) Meng, F.; Zhang, S.; Ma, L.; Zhang, W.; Li, M.; Wu, T.; Li, H.; Zhang, T.; Lu, X.; Huo, F.; Lu, J. Construction of Hierarchically Porous Nanoparticles@Metal-Organic Frameworks Composites by Inherent Defects for the Enhancement of Catalytic Efficiency. *Adv. Mater.* **2018,** *30*, 1803263.

(17) Obaidullah, M.; Furusawa, T.; Siddiquey, I. A.; Bahadur, N. M.; Sato, M.; Suzuki, N. A Fast and Facile Microwave Irradiation Method for the Synthesis of $ZnO@ZrO_2$ Core-Shell Nanocomposites and the Investigation of Their Optical Properties. *Adv. Powder Technol.* **2018,** *29*, 1804-1811.